ARTICLE

JAAS
www.rsc.org/jaas

Novel setup for investigation of the plasma conditions in direct sample insertion inductively coupled plasma atomic emission spectrometry (DSI-ICP-AES)†

Andy W. K. Cheung and Wing-Tat Chan*

Department of Chemistry, The University of Hong Kong, Pokfulam Road, Hong Kong SAR, China. E-mail: wtchan@hku.hk; Fax: +852-2857-1586; Tel: +852-2859-2156

Received 20th January 2004, Accepted 5th April 2004
First published as an Advance Article on the web 2nd August 2004

Insertion of a sample probe into the inductively coupled plasma (ICP) for direct sample insertion (DSI) could change the plasma excitation conditions. In this study, a novel setup is proposed for the investigation of the probe effects. A hollow graphite tube was used as a stand-in for the DSI sample probe to exert probe effects on the plasma. Laser-ablated testing elements (Fe, Zn and Mg) were introduced separately into the central channel of the plasma *via* the hollow graphite tube for measurement of plasma excitation temperature and electron number density. A relatively low Ar carrier gas flow rate (0.42 L min^{-1}) was used to minimize perturbation to the plasma due to the gas flow. The study shows that the extent of reduction in plasma excitation temperature and electron number density increases with probe insertion position at all observation heights. In addition, the probe effects strongly depend on the relative distance of the observation position to the tip of the probe. The probe effects are the strongest near the tip of the probe and reduce at observation positions further away from the tip. Signal-to-background ratios (SBR) of the testing elements also depend strongly on the probe insertion position and the relative distance of the observation position to the tip of the probe. The SBR peaks at 5–10 mm above the tip of the sample probe. The vertical profile of SBR depends on analyte diffusion in the plasma and the plasma excitation conditions.

1 Introduction

Direct sample insertion (DSI) is an alternative sample introduction technique for inductively coupled plasma atomic emission spectrometry (ICP-AES) and mass spectrometry (ICP-MS). A sample probe carrying a small quantity of liquid or solid is inserted into the ICP through the inner tube of the ICP torch for sample vaporization, atomization, excitation, and/or ionization. Since the first report of DSI-ICP-AES by Salin and Horlick in 1979,[1] there has been continuous effort devoted to the development of DSI-ICP in the past two decades.[2,3]

Upon sample probe insertion into the plasma, the background emission intensities reduce significantly[4–6] and the plasma excitation temperature (T_{exc}) and electron number density (n_e) reduce by thousands of degrees and orders of magnitude, respectively.[7,8] In a previous study,[8] we showed that the extent of reduction in plasma excitation conditions due to sample probe insertion mainly depended on the outer diameter of the probe, regardless of the form (solid rod, solid rod with undercut, and hollow cup with undercut) and material (graphite or molybdenum) of the probe. The probe effects (represented by reduction in Zn II/Zn I ratio) increased with probe diameter.

In this report, a hollow graphite tube was used in place of the DSI sample probe for the study of the effects of probe insertion into the plasma. Instead of transient and discrete analyte introduction in conventional DSI-ICP setup, laser ablation sampling of the testing elements (Fe, Mg and Zn) was used to generate a steady mass flux of the elements. A gentle stream of Ar carrier gas was used to sweep the laser-ablated testing elements into the plasma *via* the hollow probe. The testing elements were introduced directly into the central channel of the plasma above the sample probe. Measurement of plasma conditions at any arbitrary probe insertion position using testing elements of a wide range of boiling points is, therefore, feasible. The use of a hollow probe also circumvents the need for a separate capillary and relatively high carrier gas flow rate (1 L min^{-1}) for testing element introduction that was used in a previous study.[8]

2 Experimental

The experimental setup was similar to the one described previously, except for the use of a hollow graphite probe for direct introduction of laser-ablated testing elements into the center of the plasma.[8] The schematic diagram of the experimental setup is shown in Fig. 1. The operating parameters of the instruments are summarized in Table 1. A brief description of the setup is given below.

2.1 DSI-ICP-AES

A commercial ICP-AES spectrometer (Plasmaquant 110, Carl Zeiss, Jena, Germany) was used to generate the ICP discharge (27.12 MHz, free running). The ICP torch was a modified Fassel-type torch (Glass Workshop, Department of Chemistry, University of Alberta, Canada). The inner tube of the torch was enlarged to 9.0 mm to accommodate the sample probe.[8] A He gas stream was used to prevent arcing between the plasma and the graphite sample probe during probe insertion.

The DSI device consisted of a linear translation stage with 20-cm travel, a stepper motor and a controller (Parker Hannifin, Rohnert Park, CA, USA). The sample probe can be programmed to insert into the ICP at any arbitrary vertical position. To prevent the plasma from dropping onto the inner tubes of the torch, a spring-supported Teflon plug was used to seal the base of the torch during the probe insertion process and during DSI-ICP-AES measurement with the probe in the torch (Fig. 1). The base of the torch was sealed by the plug at a probe position of −120 mm from top of load coil or above.

Hollow graphite sample probes were fabricated from

† Presented at the 2004 Winter Conference on Plasma Spectrochemistry, Fort Lauderdale, FL, USA, January 5–10, 2004.

DOI: 10.1039/b400944d

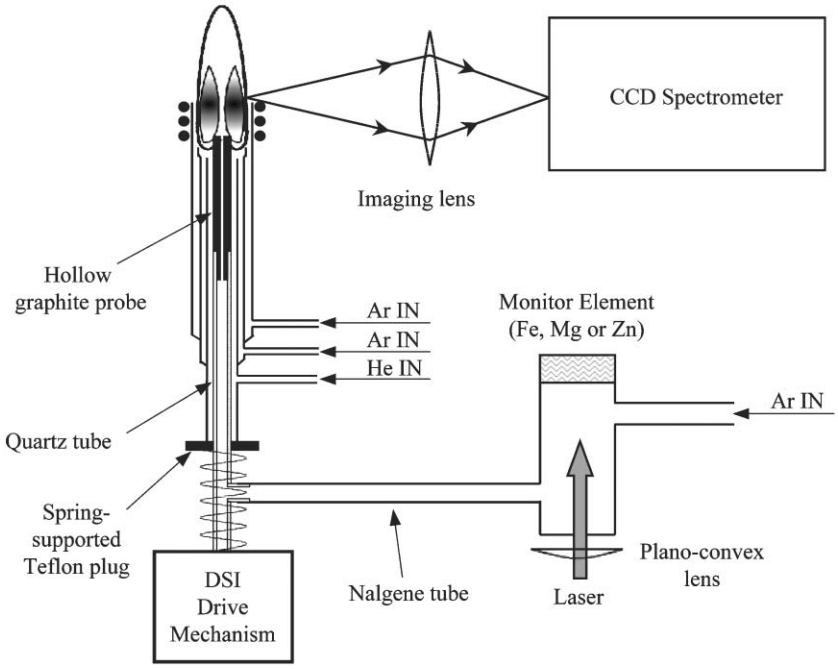

Fig. 1 Schematic diagram of the experimental setup using hollow sample probe for plasma diagnostics for DSI-ICP-AES.

Table 1 Operating parameters of the instruments

ICP	ICP forward power	1.45 kW
	Outer Ar gas flow rate	15 L min^{-1}
	Intermediate Ar gas flow rate	1.5 L min^{-1}
	Inner He gas flow rate	1.0 L min^{-1}
	Carrier Ar gas flow rate	0.42–1.42 L min^{-1}
CCD spectrometer	Entrance slit width	10 μm
	Grating density	2400 grooves per mm
	Wavelength coverage of CCD detector	~30 nm
	Observation position of CCD detector	1–37 mm HALC
	Integration time	2 s
	Replicates	3
	Number of pixels at FWHM	4–5
	Wavelength coverage at FWHM	0.12 nm
	Focal length of biconvex imaging lens	150 mm
	Diameter of biconvex imaging lens	50.8 mm
	Demagnification ratio	~5
Laser ablation system	Dimensions of metal laser targets (Fe, Zn, Mg)	12 mm × 6 mm × 2 mm
	Lens-to-metal target distance	135 mm
	Laser beam diameter	6 mm
	Laser pulse duration	6 ns
	Repetition rate	10 Hz
	Pulse energy	20–150 mJ

spectroscopic graphite rods (original length = 315 mm, diameter = 4.6 mm, CVP grade, from Morganite Special Carbons, Hampshire, UK) using a mini-lathe (Sherline Products Inc., San Marcos, CA, USA). The outer diameter of the rod was not altered. The length of the probe was 60 mm. A through hole of diameter 1.7 mm was drilled along the long axis and at the center of the probe for the transportation of laser-ablated materials into the plasma. The bottom of the probe was further machined to the form of an insert (length = 9.9 mm, outer diameter = 2.5 mm) for coupling to the quartz probe support. The probe support was a quartz tube of length 175 mm, outer diameter (od) 4.0 mm and inner diameter (id) 2.5 mm. At the lower end of the tube (5 mm from the base), a quartz side-arm (length = 5 mm, od = 4.0 mm, id = 2.5 mm) was added as the carrier gas inlet. The base of the quartz probe support was glued onto a metal block that was, in turn, attached to the translation stage of the DSI device.

The opening of the hollow probe (id = 1.7 mm) is relatively small, comparable to the size of the injector of standard ICP torches (id = 1–2 mm). The small opening produces a gas stream of relatively high linear velocity at modest volumetric flow rate (0.4 L min^{-1} in this study) so that the carrier gas can overcome the magnetohydrodynamic thrust velocity of the plasma[9] and the laser-ablated testing elements can penetrate into the ICP at probe position below the bottom of the ICP discharge.

To measure plasma emissions along the vertical axis of the ICP simultaneously, the original Echelle grating spectrometer of the ICP that can only observe the ICP at one observation height at a time was replaced with a 0.3-m CCD imaging spectrometer (SpectraPro-300i, Acton Research Corporation, MA, USA). The spectrometer was equipped with an 1100 × 330-pixels charge coupled device (CCD) detector (TEA/CCD-1100PF, Princeton Instruments, Inc., Trenton, NJ, USA). A 2-inch bi-convex converging lens (focal length = 150 mm) was used to image the plasma onto the entrance slit of the CCD spectrometer. A neutral density filter (Product Number: FSQ-ND10, Newport, CA, USA) was placed between the ICP and

the focusing thin lens to attenuate the plasma emission intensity at the CCD detector and thus prevent saturation of the detector. Analyte emissions from vertical positions of 1–37 mm height above the load coil (HALC) were collected simultaneously. Emission intensities at 3–25 mm HALC were used in this study. Plasma emissions from vertical positions below 3 mm HALC and above 25 mm HALC were blocked by the ICP torch and the observation window of the ICP torch box, respectively. Off-peak background correction was used in this study. Intensities of all pixels of the spectral peak were integrated. The background intensity was estimated from the integrated intensity of the same number of pixels adjacent to the spectral peak.

2.2 Laser sampling of testing elements

A Nd:YAG laser (Surelite II-10, Continuum, Santa Clara, CA, USA) with optical frequency doubling (wavelength = 532 nm) was used to ablate the testing elements. Metallic testing elements were used (Table 1): iron (99.5%), zinc (99.95%) (Goodfellow Metals, Cambridge, UK) and magnesium (99.9%) (Alfa Aesar, Ward Hill, MA, USA). The laser was focused loosely onto the metal targets using a plano-convex UV-grade fused silica lens (focal length = 150 mm). An iris (diameter = 3 mm) was placed in front of the focusing lens to reduce the laser pulse energy during laser ablation sampling of Zn and Mg so as to reduce the quantity of the ablated materials and prevent the CCD detector from being saturated. The laser power density on the metal targets was $\sim 10^9$ W cm^{-2}.

2.3 Procedures

Metal targets (Fe and Zn, or Fe and Mg) were placed side-by-side in the laser ablation chamber. For each set of experiments, each metal target was ablated for 1 min before probe insertion to pre-condition the target surface. For each experiment (with variation in Ar carrier gas flow rate and/or probe insertion position), the Fe target was firstly ablated for 30 s. The ICP emission intensities of Fe attained a steady state value after the first 15 s of laser ablation. Fe emission intensities were integrated using the CCD detector during the next 15 s of laser ablation (integration time = 2 s, repetitions = 3, see Table 1). The Zn or Mg target was then ablated and the ICP emission intensities were measured in the same manner.

To investigate the effect of carrier gas flow rate on plasma excitation conditions, the flow rate was varied from 0.42 L min^{-1} to 1.42 L min^{-1} at an interval of 0.08 L min^{-1}. The sample probe was inserted at 2 mm HALC throughout the experiment. The vertical emission intensity profiles of Fe and Mg along the ICP central channel were measured separately using the CCD spectrometer at each flow rate. An optimum gas flow rate that exerts minimum disturbance on the plasma excitation conditions and is yet able to entrain the laser-sampled testing elements efficiently for transport into the plasma was chosen for the study of the effects of probe insertion into the plasma.

For the study of probe effects on plasma excitation conditions and DSI-ICP-AES analytical performance, sample probe insertion positions of −22 to +10 mm HALC, at a 2 mm interval, were used. (At probe position of −22 mm HALC, the tip of the sample probe was just beneath the plasma, *i.e.*, the probe was not inserted into the plasma.) The carrier Ar gas flow rate was fixed at 0.42 L min^{-1}. The vertical emission intensity profiles of Fe and Zn along the ICP central channel were measured.

3 Results and discussion

In this paper, the effects of sample probe insertion on plasma excitation temperature and electron number density were studied. The ICP excitation temperature was estimated from the slope of the Boltzmann plot of five Fe I lines.[10] Table 2 lists the Fe I emission lines used in this study. Assuming local thermodynamic equilibrium (LTE), the electron number density can be determined from the ratio of ionic-to-atomic spectral emission intensity of a testing element.[11] Both Mg and Zn ionic-to-atomic line intensity ratios were used in this study. The Mg II/Mg I ratio was used in the study of the effects of Ar carrier gas flow rate on plasma excitation conditions. The Zn II/Zn I ratio was used in the study of the effects of probe insertion position. The sensitivity (change in ionic-to-atomic line ratio *versus* change in excitation temperature and/or electron number density) of the line pairs was approximately the same.[12] The wavelengths and spectroscopic constants of the spectral lines used are given in Table 2.

3.1 Effects of carrier Ar gas flow rate on plasma excitation conditions in DSI-ICP-AES

In this study, laser-ablated materials of Fe and Mg were carried to the ICP by a stream of Ar gas for the measurement of plasma excitation conditions. A central channel gas stream is not used in the typical DSI experimental setup. In DSI, the analyte simply vaporizes into the ICP as the sample probe heats up. The use of an Ar gas stream in the present setup may, therefore, introduce additional disturbance to the plasma excitation conditions. The extent of the effects of the additional Ar flow on plasma excitation conditions is reported below. The goal of the study is to select a gas flow rate for the investigation of the effects of probe insertion on plasma excitation conditions in the next section. The gas flow rate must have minimal effects on plasma excitation conditions and yet is sufficiently high to overcome the magnetohydrodynamic thrust velocity of the plasma at probe insertion position below the ICP discharge.

Table 2 Wavelength and spectroscopic constants of spectral lines

Element	Wavelength (λ)/nm	Statistical weight (degeneracy) of the upper energy level (g)	Einstein transition probability (A)/10^8s^{-1}	Excitation potential/eV	Ionization potential/eV
Fe I	371.994	11	0.162	3.33	
Fe I	375.823	7	0.634	4.25	
Fe I	381.584	7	1.3	4.73	
Fe I	382.046	9	0.668	4.10	
Fe I	385.991	9	0.097	3.21	
Zn I	213.856	3	7.039	5.80	
Zn II	206.200	4	3.290	6.01	9.394
Zn II	202.548	2	3.332	6.12	9.394
Mg I	285.213	3	5.086	4.35	
Mg II	280.270	2	2.616	4.42	7.646
Mg II	279.553	4	2.685	4.43	7.646

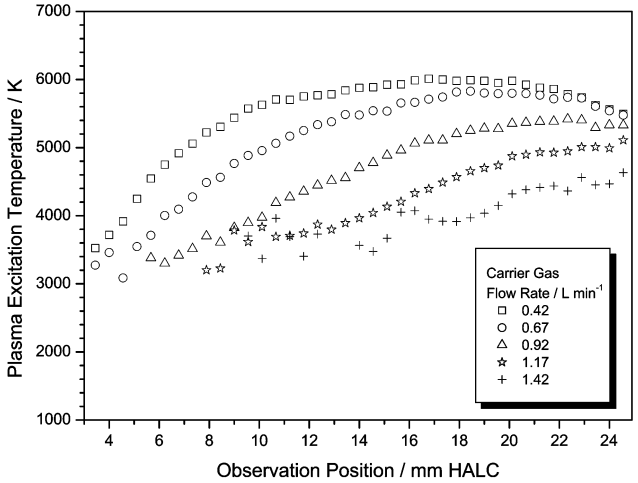

Fig. 2 Vertical profiles of plasma excitation temperature for carrier gas flow rate of 0.42–1.42 L min^{-1}. Probe insertion position was +2 mm HALC.

Figs. 2 and 3 show the vertical profiles of plasma excitation temperature and electron number density over a range of Ar carrier gas flow rate, respectively. The tip of the hollow graphite probe was positioned at 2 mm HALC. The gas flow rate was varied from 0.42 to 1.42 L min^{-1} and increased at an interval of 0.083 L min^{-1}. (Some profiles are not presented for clarity.) A gas flow rate lower than 0.42 L min^{-1} can be used in principle as the probe is inside the plasma and a high gas speed is not needed to overcome the magnetohydrodynamic thrust velocity of the plasma. However, a gas flow rate of 0.42 L min^{-1} is the minimum to overcome the thrust of the plasma when the probe is not inserted into the plasma (at −22 mm HALC or below). The upper limit of 1.42 L min^{-1} was selected because the signal-to-background ratios (SBR) of Fe I emission lines decreases quickly with gas flow rate and the SBR drops to zero for an observation position of 5 mm HALC at a gas flow rate >1.42 L min^{-1}. A general trend of excitation temperature (T_{exc}) and electron number density (n_e) *versus* vertical position of the ICP is observed for all gas flow rates. T_{exc} and n_e increase initially with observation position, reach a maximum, and roll off at higher positions. The general trend of the plasma excitation conditions is similar to the trends that are reported previously.[8] The initial lower T_{exc} and n_e at a position close to the tip of the probe are mainly an effect of gas dynamics. The probe blocks the hot plasma gas from the core and creates a region of lower T_{exc} and n_e immediately above the probe. At higher positions, the hot plasma gas merges into the central channel and increases T_{exc} and n_e to a maximum before the plasma is cooled again by the surrounding atmosphere.

Despite the similarity in the shape of vertical profiles between T_{exc} and n_e for all carrier gas flow rates studied (Figs. 2 and 3), the gas flow changes the profiles in two respects. The position of maximum T_{exc} and n_e increases with gas flow rate. For gas flow rates >1 L min^{-1}, a maximum is not observed. Instead, T_{exc} and n_e increase monotonically with observation position, probably because the maximum is located outside the upper limit of the observation window of 25 mm HALC. In addition, both T_{exc} and n_e decrease as the Ar carrier gas flow rate increases for all observation positions. For example, at a typical observation position of 15 mm HALC and carrier gas flow rate of 0.42 L min^{-1}, the excitation temperature and electron number density were 5900 K and 3×10^{13} cm^{-3}, respectively. Temperature and electron number density dropped to 3700 K and 2×10^{10} cm^{-3}, respectively, at a carrier gas flow rate of 1.42 L min^{-1}. The excitation temperature was reduced by 37% and the electron number density was reduced by 3 orders of magnitude for an approximately 3-fold increase in carrier gas flow rate. Therefore, the carrier Ar gas flow rate is critical to the plasma excitation conditions. The effects of gas flow rate are similar to the general trend observed for conventional ICP-AES using a torch with an injector that is not inserted into the plasma.[13]

Excitation temperature (T_{exc}) is plotted against carrier gas flow rate in Fig. 4 for observation positions of 5, 10, 15, 20, and 25 mm HALC. Again, the tip of the hollow graphite probe was positioned at 2 mm HALC. T_{exc} changes slowly with carrier gas flow rate at higher observation positions (20 and 25 mm HALC), probably due to more extensive mixing of the carrier gas and the plasma gas at higher position. More importantly for this study, for all observation heights, the rate of change in T_{exc} increases non-linearly with carrier gas flow rate. The rate of change in T_{exc} is relatively small at lower gas flow rate of 0.4 to 0.6 L min^{-1} (0.4–0.9 L min^{-1} for 25 mm HALC). Electron number density (n_e) follows the same pattern. The trend indicates that a carrier gas flow rate of 0.4 or 0.5 L min^{-1} is preferred in subsequent probe effects studies because of the smaller disturbance in plasma excitation conditions. Gas flow rate of 0.42 L min^{-1} will be used in the following sections.

In Figs. 2 and 3, profiles of excitation temperature and electron number density show a large fluctuation at a flow rate of 1 L min^{-1} or above. No data were obtained for an observation position of 5 mm HALC at a gas flow rate of >0.8 L min^{-1} (see also Fig. 4). The uncertainty in temperature and electron number density measurement was mainly because of significant reduction in Fe I emission intensity with gas flow rate, especially at lower observation positions (10 mm HALC or

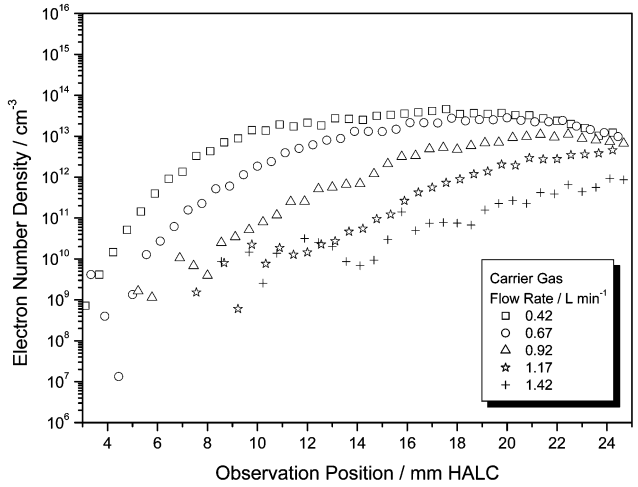

Fig. 3 Vertical profiles of electron number density for carrier gas flow rate of 0.42–1.42 L min^{-1}. Probe insertion position was +2 mm HALC.

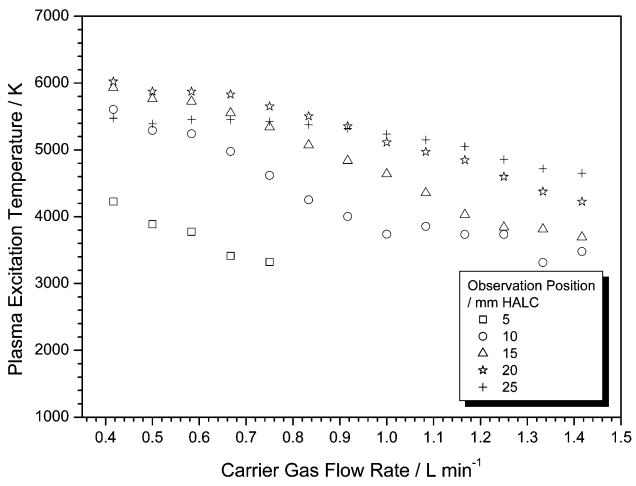

Fig. 4 Plasma excitation temperature *versus* gas flow rate. Probe insertion position was +2 mm HALC.

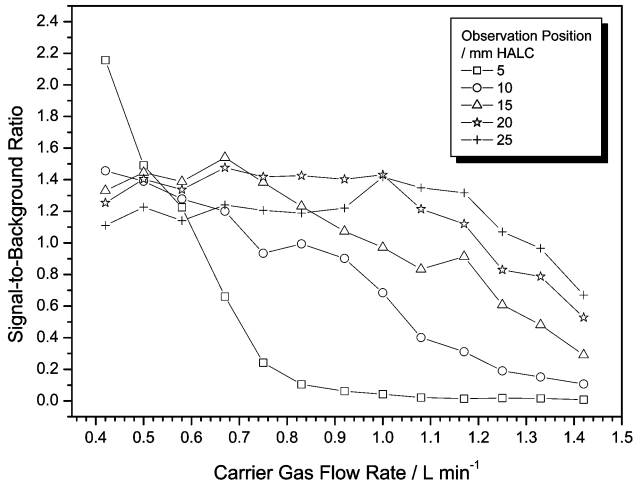

Fig. 5 Signal-to-background ratio (SBR) of Fe I 371.994 nm *versus* gas flow rate. Probe insertion position was +2 mm HALC.

below). The signal-to-background ratio (SBR) of Fe I 371.994 nm *versus* carrier Ar gas flow rate at selected observation heights is shown in Fig. 5. The SBR decreases quickly as the flow rate of carrier Ar gas increases. At a typical observation height of 15 mm HALC, the SBR of Fe I decreases by a factor of approximately 4 in the range of flow rate used. At an observation height of 5 mm HALC, the SBR of Fe I emission approaches zero at gas flow rate >0.8 L min^{-1}. The same trend is also observed for other Fe I lines.

To further evaluate the effect of gas flow rate on plasma excitation conditions, gas flow rates of 0.17 and 0.42 L min^{-1} and probe insertion positions of −16, −2 and +10 mm HALC were used (Fig. 6). From Fig. 4 it is possible to extrapolate the effects of gas flow rate on plasma excitation temperature and predict that gas flow rate of 0.17 L min^{-1} would reduce excitation temperature by a smaller extent. The study, however, is still worthwhile for the understanding of the extent of the effect of gas flow rate at different probe insertion positions. A gas flow rate of 0.17 L min^{-1} is selected because it is the bare minimum carrier gas flow rate to carry the laser-ablated materials to the ICP. The flow rate, however, is too low to punch through the plasma when the probe is positioned below the bottom of the plasma (−22 mm HALC or below). Fig. 6 shows the vertical profiles of plasma temperature for the combination of probe insertion positions and gas flow rates. At a probe insertion position of −16 mm HALC, the vertical excitation temperature profiles for the two gas-flows effectively overlap. The profile for a gas flow of 0.17 L min^{-1} shows larger fluctuation, probably because of inefficient transport of the laser ablated materials by the slow gas stream. The signal-to-background ratio (SBR) of Fe I 371.994 nm is approximately 3 times lower for gas flow of 0.17 L min^{-1} *versus* 0.42 L min^{-1}. At a probe position of −2 mm HALC, there is a greater difference in temperature for the two gas flow rates (Fig. 6). The largest difference in temperature (approximately 600 K) was found at an observation position close to the tip of the probe (3 mm HALC). There is no difference in temperature at an observation position of 12 mm HALC or above. Overall, the effect of gas flow rate is relatively small compared with the effect of sample probe insertion. At an observation position of 3 mm HALC, the excitation temperature reduces by approximately 3000 K when the probe is inserted from −16 mm to −2 mm HALC. Similarly, for an insertion position of +10 mm HALC, the reduction in excitation temperature due to probe insertion is much larger than the reduction related to gas flow rate. Gas flow effect is relatively insignificant as compared with the probe effect. The same conclusion can be drawn for electron number density measurement. Therefore, in the following sections, a carrier gas flow rate of 0.42 L min^{-1} was used for the study of probe effects on plasma excitation conditions. Despite the effects of gas flow rate, the much more prominent effects of probe insertion on plasma excitation conditions should still be possible to be demonstrated unambiguously using the present setup.

3.2 Effect of probe insertion on plasma excitation conditions

In DSI-ICP-AES, analyte appearance time, shape (width and height) of the analyte peak, SBR, and background intensity depend on the position of the sample probe in the ICP discharge.[1–9,14–28] Generally, increasing the cup position from a lower position of the ICP (*e.g.*, below the top of the load coil) to a higher position (*e.g.*, above the top of the load coil) gives sharper and more symmetrical analyte emission peaks and, therefore, enhanced SBR. The effects of probe position on plasma excitation conditions, however, are rarely discussed in the literatures. Such study may provide additional information for the optimization of DSI measurements.

Fig. 7 shows the vertical plasma excitation temperature profiles for probe insertion position of −22 mm (just before probe insertion) to +10 mm HALC. (The experiment was carried out with increment in insertion position of 2 mm. Some profiles are not shown for clarity.) The carrier gas flow rate was 0.42 L min^{-1}. Insertion of the probe into the plasma at lower positions (−20 to −8 mm HALC) has little effect on plasma

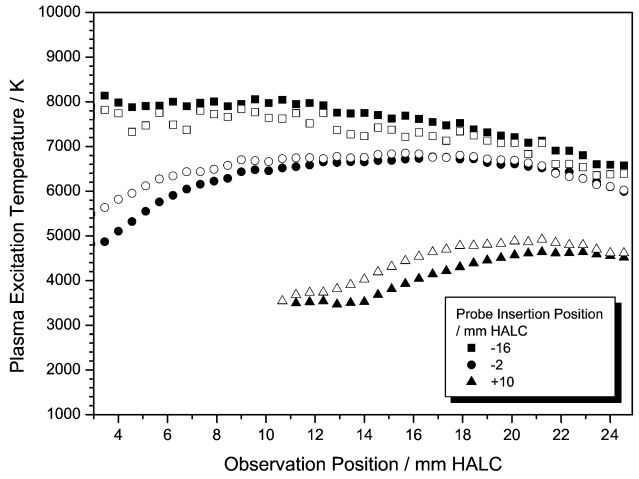

Fig. 6 Vertical profiles of plasma excitation temperature for probe insertion position of −16, −2 and +10 mm HALC. Filled symbols: carrier gas flow rate = 0.42 L min^{-1}. Hollow symbols: 0.17 L min^{-1}.

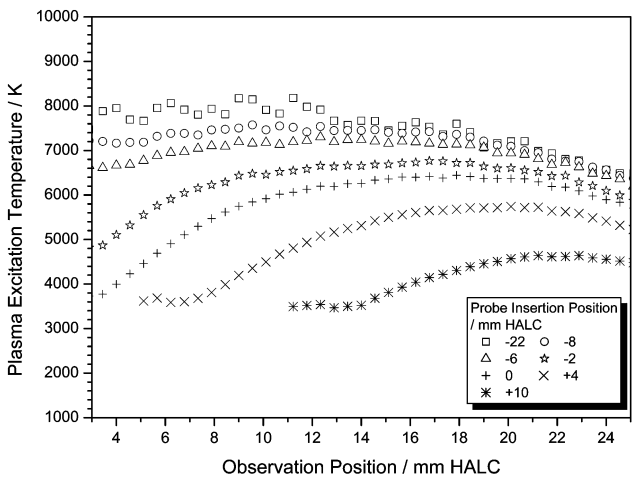

Fig. 7 Vertical profiles of plasma excitation temperature for probe insertion position of −22 to +10 mm HALC. Gas flow rate was 0.42 L min^{-1}.

excitation temperature. The temperature and general shape of the vertical temperature profile are similar to those of the plasma without probe insertion (probe position of −22 mm HALC). The excitation temperature is relatively constant at observation positions of 3–15 mm HALC and the temperature reduces monotonically at higher plasma positions. Excitation temperature, however, reduces, albeit slowly, with increasing probe position. The temperature decreases from 7900 K to 7300 K as the probe position increases from −22 mm to −8 mm HALC at an observation position of 5 mm HALC, and 7700 K to 7500 K at 15 mm HALC (Fig. 8). Compared with the uncertainty in temperature estimation of 200 K,[8] the reduction in temperature due to probe insertion is relatively minor for a probe position below −8 mm HALC.

At a probe insertion position of −6 mm HALC or above, the shape of the vertical temperature profile changes significantly. A maximum appears and the position of the maximum increases with probe insertion position (Fig. 7). The plasma temperature also reduces quickly with increasing probe position (Figs. 7 and 8). As discussed in the previous section, the maximum in the vertical temperature profile is a result of gas dynamics. Interestingly, the effect is prominent at a conventional insertion position of 0 mm HALC. Temperature reduces to 4500 K and 6300 K at observation positions of 5 mm and 15 mm HALC, respectively.

For an insertion position of 4 mm HALC or above, the excitation temperature is approximately 3500 K at the tip of the probe for all insertion positions (Fig. 7). In addition, the temperature is relatively constant from the tip of the probe to approximately 2 mm above the probe. The temperature starts to increase at a higher position relative to the probe as the carrier gas is heated by the surrounding hot plasma gas. The relatively flat temperature profile at 0–2 mm above the tip of the probe probably represents the temperature of the carrier gas exiting the heated sample probe. The probe may reach a temperature of 3500 K in the plasma.

The effects of sample probe insertion on electron number density are similar to that of the excitation temperature (Figs. 9 and 10). Again, at low sample probe insertion positions (−22 to −8 mm HALC), electron number density is relatively constant at observation positions of 3–15mm HALC. Electron number density decreases with observation position at 15 mm HALC or above (Fig. 9). As the probe was inserted from −22 to −8 mm HALC, electron number density varied from 7×10^{14}cm^{-3} to 2×10^{14} cm^{-3} at an observation position of 5 mm HALC and 3×10^{14}cm^{-3} to 4×10^{14}cm^{-3} at 15 mm HALC. Assuming a 200 K uncertainty in the temperature of the plasma, the uncertainty in electron number density is a factor of 2.[8] The probe effects are relatively minor for probe positions of

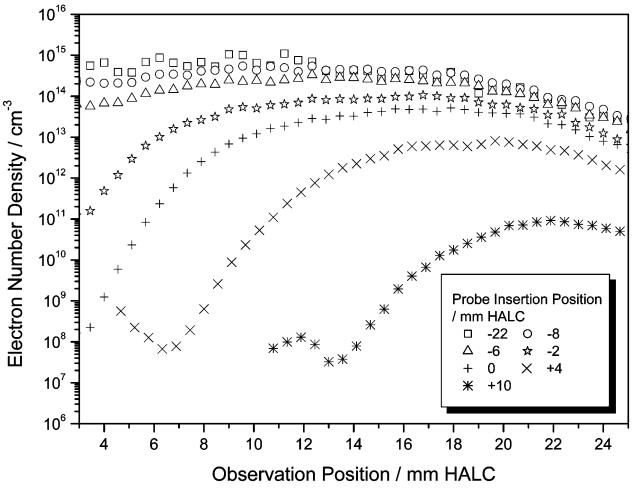

Fig. 9 Vertical profiles of electron number density for probe insertion position of −22 to +10 mm HALC. Gas flow rate was 0.42 L min^{-1}.

−22 mm to −8 mm HALC. At higher insertion positions (−6 mm HALC or above), the electron number density decreases rapidly by orders of magnitude.

The tremendous decrease in excitation temperature and electron number density for probe positions of −6 mm HALC or above would reduce the efficiency of analyte atomization and excitation significantly (Figs. 7 and 9). In addition, excitation temperature and electron number density increase with distance from the tip of the probe and reach a maximum a few centimetres above the probe (Figs. 7 and 9). The signal-to-background ratio (SBR) of an analyte should increase with observation position relative to the tip of the probe to reach a maximum before reducing again. Fig. 11 shows the normalized SBR vertical profiles of Fe I 371.994 nm for a probe insertion position of −2 to 10 mm HALC. The data are derived from the same set of experiments as Fig. 7. Normalized SBR of Fe I 371.994 nm were used to emphasize the constant offset in SBR maximum against probe insertion position. The maximum SBR is approximately 10 for all insertion positions above −2 mm HALC. SBR for lower insertion positions (−4 mm HALC or below) are much smaller (approximately 1–2) because the observed region corresponds to the tail of the SBR profile. Same trend is observed for other Fe I lines. In Fig. 11, a maximum in SBR was indeed observed. However, maximum SBR does not occur at the same position of the corresponding maxima of excitation temperature and/or electron number density. The SBR maximum is approximately 5 mm above the tip of the sample probe for all insertion

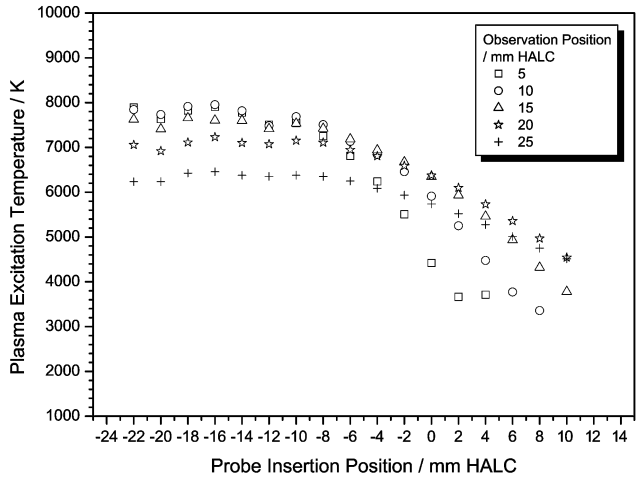

Fig. 8 Plasma excitation temperature *versus* probe insertion position. Gas flow rate was 0.42 L min^{-1}.

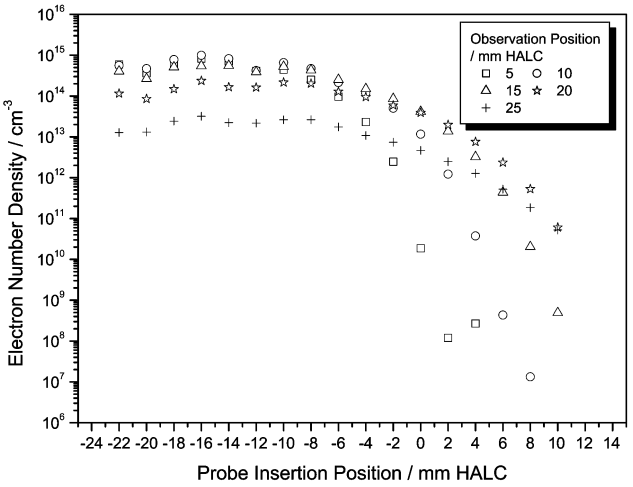

Fig. 10 Electron number density *versus* probe insertion position. Gas flow rate was 0.42 L min^{-1}.

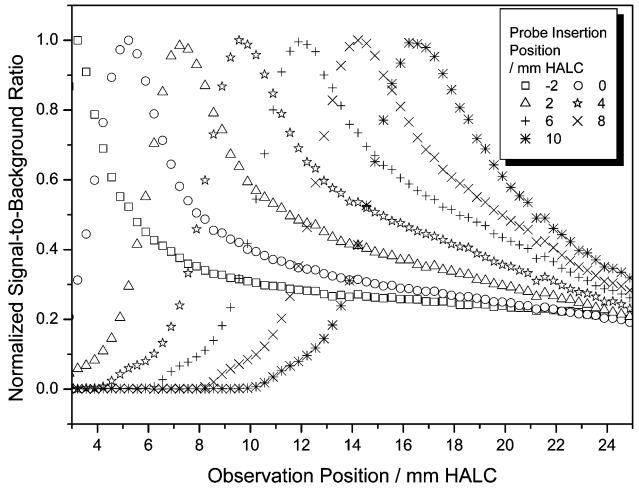

Fig. 11 Vertical profiles of normalized signal-to-background ratio of Fe I 371.994 nm for probe insertion position of −2 to +10 mm HALC.

positions. A possible mechanism for the constant offset of maximum SBR from the probe is that there exists a balance between reduction in analyte particle density due to diffusion of analyte atoms from the ICP central channel and increase in excitation conditions with relative distance from the tip of the probe. As the plume of analyte atoms ascends from the sample probe, the cross sectional area of the plume increases due to analyte diffusion. The plume assumes the form of an inverted cone (Fig. 12). Fig. 12 shows the emission of Ba for probe insertion at 6 mm HALC and carrier gas flow rate of 0.42 L min^{-1}. The inverted cone of emission has an apex angle of approximately 30°.

The normalized SBR profiles of Zn II 202.548 nm are shown in Fig. 13. Maximum SBR of Zn II 202.548 nm occurs at 8–12 mm above the tip of the probe for an insertion position of +10 to −2 mm HALC, respectively (Fig. 13). The normalized SBR profiles of Zn I 213.856 nm show the same trend. The offset in maximum SBR from the tip of the probe is slightly smaller for Zn I 213.856 nm (7–10 mm) for the same insertion positions. Compared with the Fe I lines (Fig. 11), the SBR

Fig. 12 Image of the ICP with sample probe insertion showing the inverted cone of Ba emission at the tip of the sample probe. Sample probe diameter was 4.6 mm. Opening of the probe was 1.7 mm. Probe insertion position was 6 mm HALC. Carrier Ar gas flow rate was 0.42 L min^{-1}.

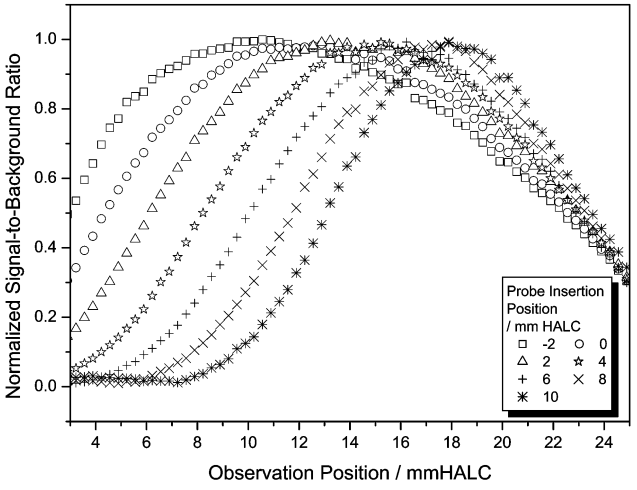

Fig. 13 Vertical profiles of normalized signal-to-background ratio of Zn II 202.548 nm for probe insertion position of −2 to +10 mm HALC.

maximum occurs at a higher position relative to the tip of the probe for the Zn lines, probably because of the higher excitation potential of the Zn lines. The position of maximum SBR of Fe and Zn emissions (Fe I < Zn I < Zn II) corresponds to the excitation potentials of the emission lines (3.33, 5.80 and 6.12 eV, for Fe I, Zn I and Zn II, respectively). The relative distance from the tip of the probe also reflects the duration for plasma–analyte interaction. Figs. 11and 13 show that the optimum observation position of DSI-ICP-AES measurement depends on probe insertion position and the excitation potential of the analyte emission lines.

4 Conclusions

A novel setup has been used to investigate the plasma conditions in DSI-ICP-AES. Carrier gas flow rate can change the plasma excitation conditions significantly. A relatively low carrier gas flow rate (0.42 L min^{-1}) was used to minimize perturbation to the plasma. In agreement with previous work, probe insertion into the plasma reduces the plasma excitation temperature and electron number density significantly. In addition, the analyte vertical emission profile depends on the probe position. The observation position of the plasma for maximum SBR depends on the probe insertion position and excitation potential of the analyte.

In the current study, the probe effects on plasma excitation conditions along the central channel of the plasma were studied using a relatively large probe (od = 4.6 mm). A smaller probe should exert smaller effects on the plasma excitation conditions. The scope of the measurement can possibly be expanded to the study of the plasma conditions at any vertical and radial position of the plasma simply by placing a small probe at the interested position. Also, it would be more convenient to study the initial processes of analyte–-plasma interaction that occur mainly at the load coil region by placing the probe at a more convenient position, *e.g.*, at 0 mm HALC. The applicability of the probe method for plasma diagnostics will be pursued in future study.

Acknowledgements

This work was supported by the Hong Kong Research Grant Council under Grant No. HKU 7097/00P.

References

1 E. D. Salin and G. Horlick, *Anal. Chem.*, 1979, **51**, 2284.
2 R. Sing, *Spectrochim. Acta, Part B*, 1999, **54**, 411.

3 V. Karanassios and G. Horlick, *Spectrochim. Acta Rev.*, 1990, **13**, 89.
4 M. Umemoto and M. Kubota, *Spectrochim. Acta, Part B*, 1987, **42**, 491.
5 G. F. Kirkbright and S. J. Walton, *Analyst*, 1982, **107**, 276–281.
6 D. Sommer and K. Ohls, *Fresenius' J. Anal. Chem.*, 1980, **304**, 97–103.
7 W. T. Chan, G. C.-Y. Chan, Z.-B. Gong and N. M.-N. Fan, *Anal. Sci.*, 2000, **16**, 235–239.
8 G. C.-Y. Chan, N. M.-N. Fan and W. T. Chan, *Spectrochim. Acta, Part B*, 2001, **56**, 13–25.
9 M. Umemoto and M. Kubota, *Spectrochim. Acta, Part B*, 1991, **46**, 1275–1284.
10 J. M. Mermet in *Inductively Coupled Plasma Emission Spectroscopy—Part 2*, ed. P. W. J. M. Boumans, Wiley-Interscience, New York, USA, 1987, ch. 10, pp. 356–373.
11 M. W. Blades in *Inductively Coupled Plasma Emission Spectroscopy—Part 2*, ed. P. W. J. M. Boumans, Wiley-Interscience, New York, USA, 1987, ch. 11, pp. 387–420.
12 G. C.-Y. Chan, W. T. Chan, X.-L. Mao and R. E. Russo, *Spectrochim. Acta, Part B*, 2000, **55**, 221–235.
13 I. Novotny, J. C. Farinas, J. L. Wan, E. Poussel and J. M. Mermet, *Spectrochim. Acta, Part B*, 1996, **51**, 1517–1526.
14 V. Karanassios and T. J. Wood, *Appl. Spectrosc.*, 1999, **53**, 197–204.
15 X. R. Liu and G. Horlick, *J. Anal. At. Spectrom.*, 1994, **9**, 833–840.
16 W. E. Pettit and G. Horlick, *Spectrochim. Acta, Part B*, 1986, **41**, 699–712.
17 W. T. Chan and G. Horlick, *Appl. Spectrosc.*, 1990, **44**, 380–390.
18 V. Karanassios, G. Horlick and M. Abdullah, *Spectrochim. Acta, Part B*, 1990, **45**, 119–129.
19 I. B. Brenner, A. Lorber and Z. Goldbart, *Spectrochim. Acta, Part B*, 1987, **42**, 219–225.
20 G. F. Kirkbright and Zhang Li-Xing, *Analyst*, 1982, **107**, 617–622.
21 T. J. Wood and V. Karanassios, *Can. J. Anal. Sci. Spectrosc.*, 2000, **45**, 48–52.
22 G. C.-Y. Chan, N. M.-N. Fan and W. T. Chan, *J. Anal. At. Spectrom.*, 2001, **16**, 648–651.
23 N. W. Barnett, M. J. Cope, G. F. Kirkbright and A. A. H. Taobi, *Spectrochim. Acta, Part B*, 1984, **39**, 343–348.
24 G. Zaray, J. A. C. Broekaert and F. Leis, *Spectrochim. Acta, Part B*, 1988, **43**, 241–253.
25 C. D. Skinner and E. D. Salin, *J. Anal. At. Spectrom.*, 1997, **12**, 725–732.
26 M. Umemoto and M. Kubota, *Spectrochim. Acta, Part B*, 1987, **42**, 491–499.
27 V. Karanassios, G. Horlick and M. Abdullah, *Spectrochim. Acta, Part B*, 1990, **45**, 105–118.
28 C. D. Skinner and E. D. Salin, *J. Anal. At. Spectrom.*, 1997, **12**, 1131–1138.